ACS Energy LETTERS

Cite This: ACS Energy Lett. 2019, 4, 534−541

http://pubs.acs.org/journal/aelccp

LETTER

Ag-Doped Halide Perovskite Nanocrystals for Tunable Band Structure and Efficient Charge Transport

Shu Zhou,[†] Yaping Ma,[†] Guodong Zhou,[‡] Xin Xu,[‡] Minchao Qin,[†] Yuhao Li,[†] Yao-Jane Hsu,[§] Hanlin Hu,[∥] Gang Li,[∥] Ni Zhao,[‡] Jianbin Xu,[‡] and Xinhui Lu*[,†]

[†]Department of Physics, The Chinese University of Hong Kong, New Territories, Hong Kong

[‡]Department of Electronic Engineering, The Chinese University of Hong Kong, New Territories, Hong Kong

[§]National Synchrotron Radiation Research Center, Hsinchu 30076, Taiwan

[∥]Department of Electronic and Information Engineering, Hong Kong Polytechnic University, Hong Hum, Kowloon, Hong Kong

Supporting Information

ABSTRACT: Heterovalent doping of halide perovskite nanocrystals (NCs), offering potential tunability in optical and electrical properties, remains a grand challenge. Here, we report for the first time a controlled doping of monovalent Ag^+ into $CsPbBr_3$ NCs via a facile room-temperature synthesis method. Our results suggest that Ag^+ ions act as substitutional dopants to replace Pb^{2+} ions in the perovskite NCs, shifting the Fermi level down toward the valence band and in turn inducing a heavy p-type character. Field effect transistors fabricated with Ag^+-doped $CsPbBr_3$ NCs exhibit 3 orders of magnitude enhancement in hole mobility at room temperature, compared with undoped $CsPbBr_3$ NCs. Low-temperature electrical studies further confirm the influence of Ag^+ doping on the charge-carrier transport. This work demonstrates the tunability of heterovalent doping on the electrical properties of halide perovskite NCs, shedding light on their future applications in versatile optoelectronic devices.

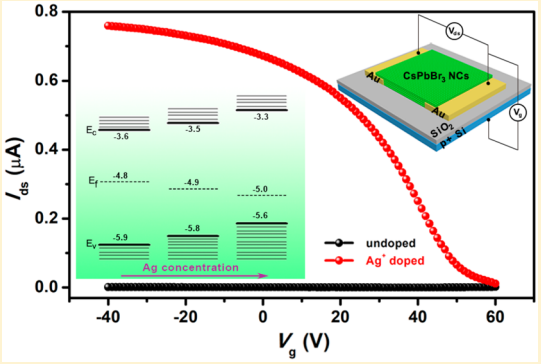

Halide perovskite, named after its crystal structure, has achieved significant success in the field of photovoltaics because of its superior optical and electrical properties, such as large optical absorption coefficients, high dual electron and hole mobility, and strong defect tolerance.[1−4] Recently, some researchers have begun to explore the material's potential applications beyond photovoltaics, such as in LEDs, phototransistors, and lasers, for which tunable optical and electrical properties are highly desirable.[5−10] Halide perovskite nanocrystals (NCs) are among the most intensively studied variants of perovskite.[11,12] Many approaches have been developed to synthesize various kinds of halide perovskite NCs with controlled size and morphology, such as hot injection,[13] ligand-assisted reprecipitation,[14] ligand-mediated transport,[15] laser ablation,[16] and electrospray techniques.[17] The external quantum efficiency (EQE) of perovskite NC-based LEDs has exceeded 11% within just a few years.[18,19] Solar cells based on halide perovskite NCs have achieved a PCE of 13.4%.[20] Applications beyond optoelectronics, such as photocatalytic CO_2 reduction and gas sensing, have also been reported.[21,22] However, very few transistor studies on perovskite NCs have been reported to date, mainly because of the limited conductivity and charge-carrier mobility.[23−25]

To meet the diverse requirements of versatile devices, the electrical and optical properties of halide perovskite NCs must be controllably and flexibly tunable. Doping, as one of the most important methods offering a lot of freedom to semiconducting materials, stands out as a feasible route.[26−28] Isovalent dopants such as Mn^{2+}, Zn^{2+}, Sn^{2+}, and Cd^{2+} were reported to be successfully doped into halide perovskite NCs to substitute the toxic Pb^{2+} and to tune the optical properties.[29−32] Heterovalent doping of halide perovskite NCs has also demonstrated great potential. Begum et al. reported doping Bi^{3+} into $CsPbBr_3$ NCs by a hot-injection method.[33] They found that Bi^{3+} doping improved the interfacial energy alignment of perovskite NCs with molecular acceptors which in turn facilitated the charge transfer at the interface. Al^{3+}-doped $CsPbBr_3$ NCs, also synthesized by hot-

Received: December 18, 2018
Accepted: January 21, 2019
Published: January 21, 2019

Downloaded via NATL TSING HUA UNIV on January 13, 2020 at 04:10:06 (UTC).
See https://pubs.acs.org/sharingguidelines for options on how to legitimately share published articles.

© 2019 American Chemical Society

DOI: 10.1021/acsenergylett.8b02478
ACS Energy Lett. 2019, 4, 534−541

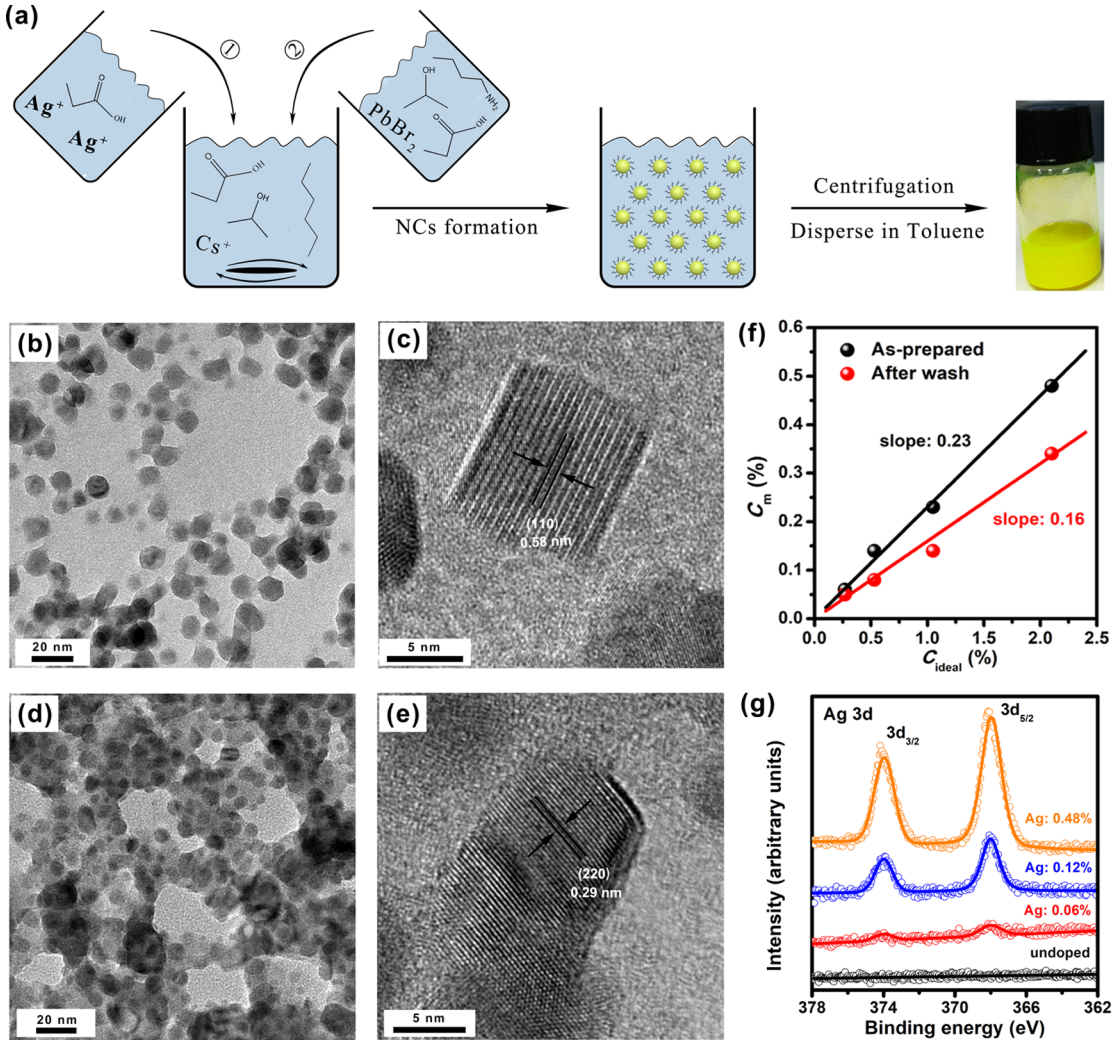

Figure 1. (a) Schematic of the room-temperature colloidal synthesis of Ag^+-doped $CsPbBr_3$ NCs. TEM images for (b) undoped and (d) Ag^+-doped $CsPbBr_3$ NCs. (c and e) Corresponding HRTEM images. (f) Ag^+ concentration measured by ICP-OES (C_m) versus the ideal concentration (C_{ideal}) calculated from the feed solution. (g) Ag 3d XPS spectra of undoped and Ag^+-doped $CsPbBr_3$ NCs.

injection, were reported to exhibit stable blue photoluminescence (PL), being a possible down-convertor material for backlit displays.[34] More recently, perovskite NCs doped with lanthanide ions have been reported to endow tunable light emissions spanning from visible to near-infrared (NIR) spectra.[35,36] In addition, Ag^+ doping has been previously demonstrated in bulk perovskite[37] and PbSe NCs.[38] Nevertheless, there is still a lack of studies on the tunability of heterovalent doping on electrical properties of perovskite NCs.

In this work, we employ a facile room-temperature approach for controlled doping of inorganic cesium lead bromide ($CsPbBr_3$) NCs with monovalent Ag^+ ions. Ultraviolet photoelectron spectroscopy (UPS) results demonstrate that the Ag^+ doping induces electronically active impurities, which induce energy levels near the valence band of $CsPbBr_3$ NCs. Therefore, the band structure of $CsPbBr_3$ NCs can be readily tuned by changing the doping concentration. In contrast to the conventional hot-injection method, this room-temperature method allows the incorporation of relatively short ligands with low boiling point. Consequently, as-synthesized $CsPbBr_3$ NCs are readily fabricated into field effect transistors (FETs) for a systematic investigation of doping-dependent electrical properties. A typical p-type transport character can be gradually tuned up with an increasing doping concentration. Field effect hole mobility surges by 3 orders of magnitude when the doping concentration increases from 0 to 0.48%. Low-temperature electrical studies further elucidate the correlation between doping and charge-carrier transport by suppressing both ion migration and phonon scattering. This work not only demonstrates a feasible heterovalent doping strategy with considerable tunability in electrical properties of $CsPbBr_3$ NCs but also reveals fundamental charge transport mechanism upon doping, paving the way for future applications of halide perovskite NCs into versatile optoelectronic devices.

The Ag^+ doping strategy was developed based on the synthesis method for undoped $CsPbBr_3$ NCs reported by Akkerman et al.[39] As depicted in Figure 1a, Cs_2CO_3 was first dissolved in propionic acid (PrAc) and then diluted in a solvent mixture of isopropanol (IPA) and hexane (HEX) to form the Cs^+ precursor. $PbBr_2$ was dissolved in a mixture of PrAc, IPA, and low-boiling-point short ligand butylamine (BuAm) to form the Pb^{2+} precursor. Undoped $CsPbBr_3$ NCs can be formed by injecting the Pb^{2+} precursor into the Cs^+ precursor. To avoid the introduction of foreign ions during the Ag^+ doping, we dissolved Ag_2CO_3 in PrAc to form the Ag^+

DOI: 10.1021/acsenergylett.8b02478
ACS Energy Lett. 2019, 4, 534−541

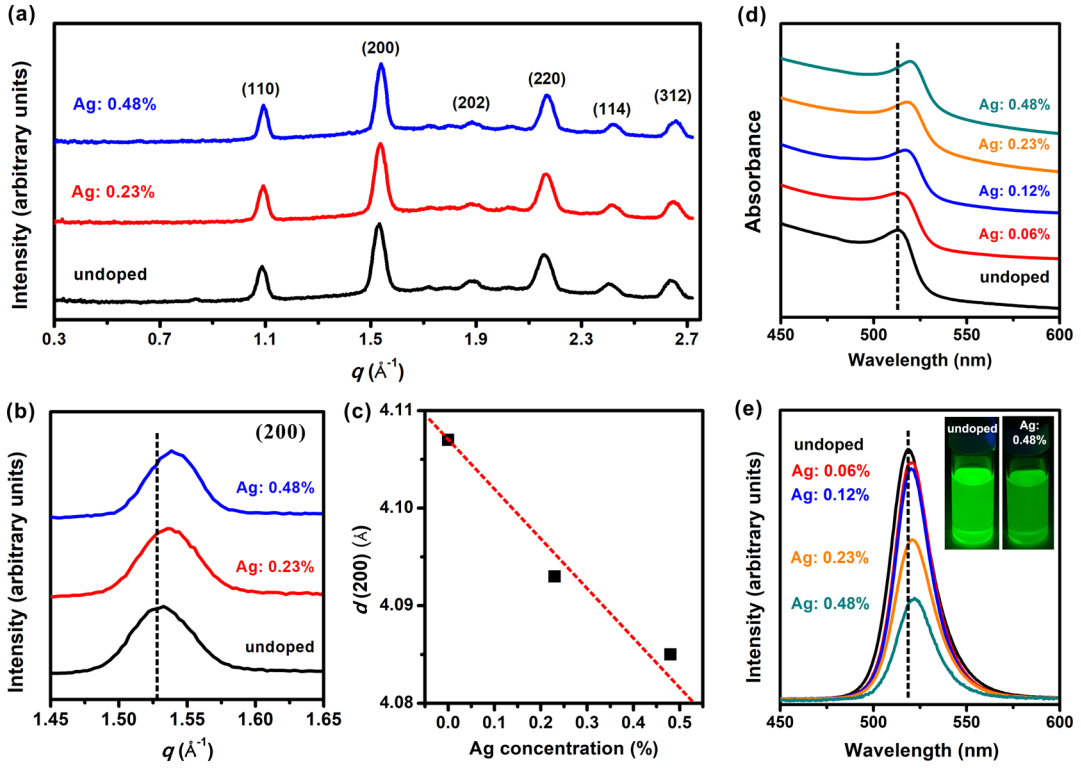

Figure 2. (a) GIWAXS intensity profiles of undoped, 0.23% Ag^+-doped, and 0.48% Ag^+-doped $CsPbBr_3$ NCs. (b) Intensity profiles of the (200) peak. (c) *d*-spacing of (200) planes versus Ag^+ doping concentration. (d) Absorption and (e) emission spectra for undoped and Ag^+-doped $CsPbBr_3$ NCs. Insets of panel e are the luminescent $CsPbBr_3$−NC colloids under UV light.

precursor. The Ag^+ precursor and Pb^{2+} precursor were then sequentially injected into the Cs^+ precursor to generate Ag^+-doped $CsPbBr_3$ NCs instantly, which were then precipitated by centrifugation and redispersed in toluene to form NC inks ready for device fabrication. The whole process was carried out at room temperature under nitrogen atmosphere in the glovebox without degassing. Figure 1b,d presents the transmission electron microscopy (TEM) images of undoped and Ag^+-doped $CsPbBr_3$ NCs synthesized at the IPA:HEX ratio of 1:2. It is found that the synthesized NCs possess a noncubic morphology, similar to what has been observed on the perovskite NCs produced from ligand-assisted reprecipitation and ligand-mediated transport methods at room temperature.[14,15] Both undoped and Ag^+-doped $CsPbBr_3$ NCs aggregate because the short and low-boiling ligands at the NC surface could not give rise to enough steric force to enable well-separated NCs.[39] There is no obvious change in the average sizes of the NCs with or without Ag^+ doping, which are both around 10 nm (Figure S1). However, the size distribution for Ag^+-doped $CsPbBr_3$ NCs appears to be broader than the undoped $CsPbBr_3$ NCs, likely because of the more serious aggregation of the NCs (Figure 1d). In addition, it is evident that the shape of the $CsPbBr_3$ NCs has changed after doping. These imply that the dopant precursor may play a role in the growth of perovskite NCs.[40] The selected area electron diffraction (SAED) images (Figure S1) and high-resolution TEM (HRTEM) images (Figure 1c,e) indicate that both undoped and doped $CsPbBr_3$ NCs have an orthorhombic crystal structure, consistent with previous reports.[39]

Inductively coupled plasma optical emission spectroscopy (ICP-OES) was utilized to characterize the correlation between the Ag^+ concentration in doped $CsPbBr_3$ NCs (C_m) and the concentration of Ag^+ in the feed solution (C_{ideal}). To confirm the existence of Ag^+ in the core of $CsPbBr_3$ NCs, all doped NC samples were washed with toluene to remove the surface adsorbed or loosely bonded dopants. It was estimated from a linear fitting of C_m versus C_{ideal} (Figure 1f) that about 16% of the Ag^+ ions in the feed solution were successfully incorporated into the $CsPbBr_3$ NCs.

Further evidence of controlled Ag^+ doping was provided by X-ray photoelectron spectroscopy (XPS). The survey scans for binding energies from 0 to 800 eV clearly show the signals of Cs, Pb, Br, O, and C for both undoped and Ag^+-doped $CsPbBr_3$ NCs (Figure S2). Compared with the XPS results of $CsPbBr_3$ NCs capped with long ligands,[33,34] our $CsPbBr_3$ NCs exhibit relatively weaker C 1s peak, demonstrating the presence of short ligands. Figure 1g shows the XPS spectra in the Ag 3d region. No peak was observed for undoped $CsPbBr_3$ NCs, as expected. When the doping concentration increases from 0.06% to 0.48%, two peaks at 367 and 374 eV, associated with the Ag $3d_{5/2}$ and $3d_{3/2}$ binding energies, intensify accordingly, signifying a successfully controlled doping.

Grazing incidence wide-angle X-ray scattering (GIWAXS) measurements were carried out to examine the influence of Ag^+ doping on the crystal structure of $CsPbBr_3$ NCs.[41] Figure 2a presents sector plots (intensity versus $|q|$) of two-dimensional (2D) GIWAXS patterns for thin films of $CsPbBr_3$ NCs with different doping concentrations. The corresponding 2D GIWAXS patterns are shown in Figure S3. The diffraction peaks agree with HRTEM results that obtained NCs are highly crystallized with an orthorhombic structure. The peak position slightly shifts to a larger q with the increase of the doping concentration (Figure 2b), suggesting that a small lattice

DOI: 10.1021/acsenergylett.8b02478
ACS Energy Lett. 2019, 4, 534−541

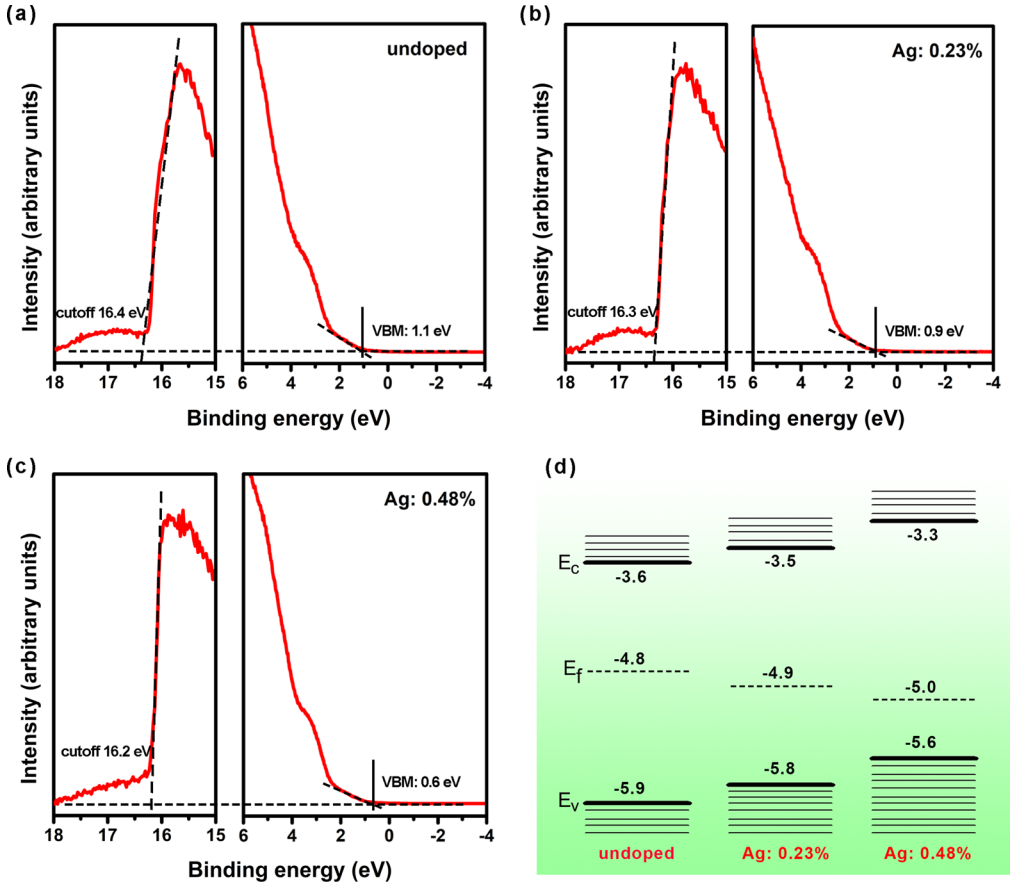

Figure 3. UPS spectra of (a) undoped and (b and c) Ag^+-doped $CsPbBr_3$ NCs. The valence-band maximum (VBM) and secondary electron edge of undoped and each Ag^+-doped $CsPbBr_3$ NC samples are indicated. (d) Illustration of band structure with the increase of Ag^+ concentration. E_c, conduction band edge; E_v, valence band edge; E_f, Fermi energy level.

contraction (Figure 2c) was induced by the incorporation of Ag^+ ions into the lattice.[30]

The optical absorption spectra of undoped and Ag^+-doped $CsPbBr_3$ NCs are shown in Figure 2d. It is seen that the first excitonic peak exhibits a tiny red-shift from ~512 nm/2.42 eV to ~519 nm/2.39 eV with the increase of doping concentration. The optical band gap (E_{opt}) estimated from the absorption edge via the Tauc plot (Figure S4) changes from ~2.35 to 2.32 eV, consistent with the shift of the excitonic transition. Figure 2e shows the corresponding PL spectra for undoped and Ag^+-doped $CsPbBr_3$ NCs. The full widths at half maxima (fwhm) of all PL peaks are found to be ~20 nm. A PL quenching was observed when the doping concentration increased, which could be ascribed to the increased nonradiative Auger recombination caused by heterovalent doping.[42,43] The PL quenching accompanied by a decrease in the PL decay lifetime (Figure S5) indicates an increase of trap states in the band gap of the $CsPbBr_3$ NCs upon Ag^+ doping, similar to the report on Bi^{3+}-doped $CsPbBr_3$ NCs.[33] In addition, the PL peak slightly shifts from ~518 nm/2.39 eV to ~522 nm/2.37 eV. The PL shift is a bit smaller than the shift of the excitonic peak in Figure 2d, suggesting a change of the Stokes shifts in $CsPbBr_3$ NCs because of the doping-induced perturbation to the band edge states or variation of the size distribution.[44,45] First-principle study on halide perovskites indicates that the Ag-4d orbital will hybridize with the Br-3p orbital, giving rise to a higher valence band edge.[46] This may lead to narrowing of the band gap in Ag^+-doped $CsPbBr_3$ NCs (Figure S6). The actual insignificant red-shift in the absorption edge and PL peaks suggests this effect could be mitigated, possibly by the doping-induced lattice contraction (Figure 2c) which usually leads to blue-shift of the PL energy in perovskite NCs.[30]

To reveal the impact of Ag^+ doping on the band structure of $CsPbBr_3$ NCs, UPS was employed to determine the valence band maximum (VBM) or Fermi level with respect to the vacuum level by calculating the difference between the excitation energy (He−I 21.2 eV) and the spectrum width or the secondary electron cutoff, respectively (Figure 3a−c). The VBM of undoped $CsPbBr_3$ NCs was calculated to be −5.9 eV, agreeing with previous reported values.[39] It gradually shifts upward upon doping (−5.8 eV for 0.27% Ag^+-doped $CsPbBr_3$ NCs and −5.6 eV for 0.48% Ag^+-doped $CsPbBr_3$ NCs), indicating the presence of dopant levels near the valence band edge. This is further evidenced by performing scanning tunneling microscopy (STM) measurements on both undoped and doped $CsPbBr_3$ NCs (Figures S6−S8). Meanwhile, the Fermi level shifts downward (−4.8 eV for undoped, −4.9 eV for 0.27%, and −5.0 eV for 0.48%). Together, it confirms that a well-established p-type doping has been achieved after Ag^+ doping, suggesting that the Ag^+ ions have been incorporated into the substitutional sites and replace Pb^{2+} ions in the perovskite NCs.[37,47,48] Although Ag^+ ions were also reported to replace the A site ions (Cs^+),[19] it is unlikely to obtain a p-type character through isovalent doping. Combining the Fermi level positions determined by UPS results and the conduction

DOI: 10.1021/acsenergylett.8b02478
ACS Energy Lett. 2019, 4, 534−541

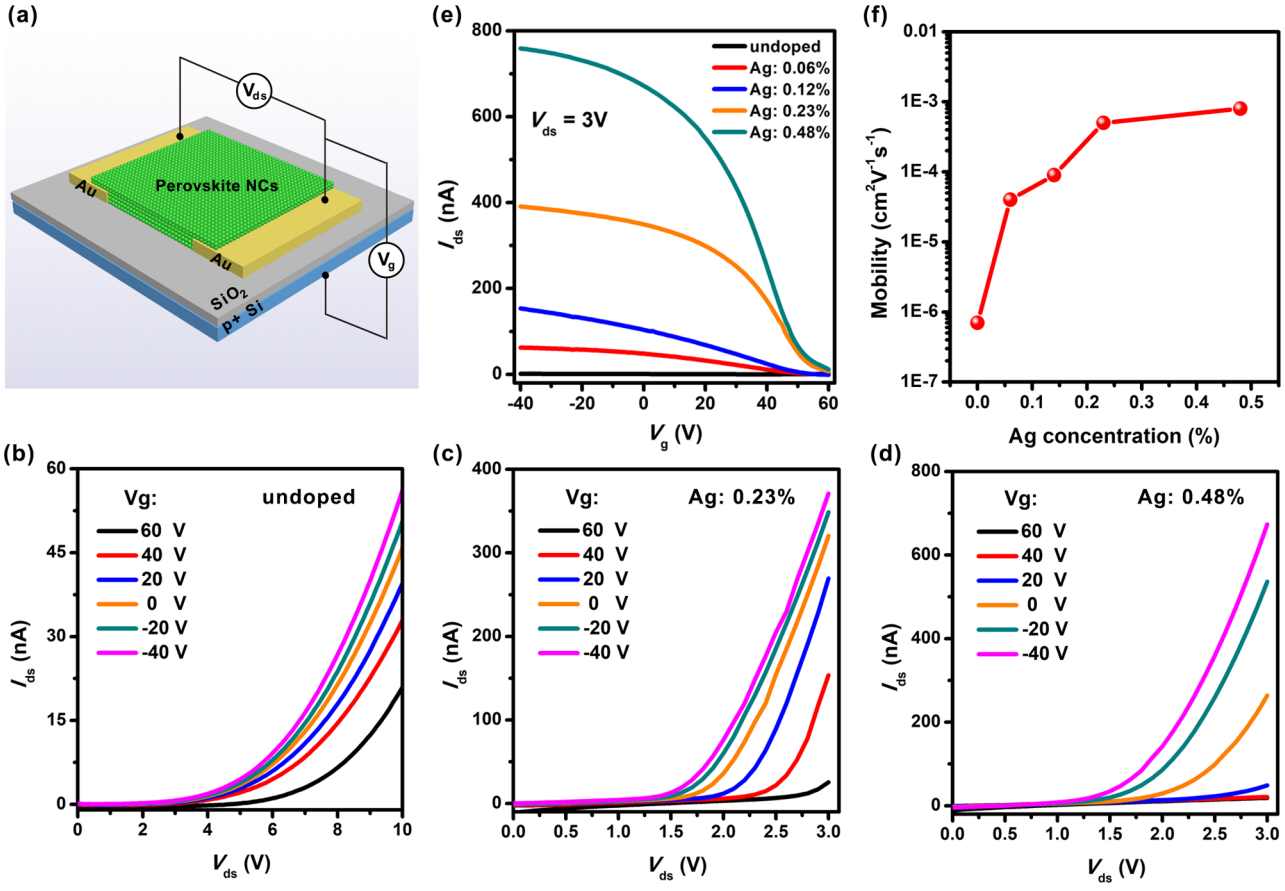

Figure 4. (a) Schematic of the bottom-gate bottom-contact $CsPbBr_3$-NC FET device structure. Output characteristics of (b) undoped, (c) 0.23% Ag^+-doped, and (d) 0.48% Ag^+-doped $CsPbBr_3$-NC FETs. (e) Transfer characteristics of the FETs fabricated with undoped and Ag^+-doped $CsPbBr_3$ NCs. (f) FET hole mobility versus Ag^+ concentration.

band minimum (CBM) deduced from the VBM and the optical band gaps (CBM = VBM + E_{opt}),[27] we illustrate the band structure of undoped and Ag^+-doped $CsPbBr_3$ NC samples in Figure 3d.

To investigate the tunability of doping on electrical properties of $CsPbBr_3$ NCs, we have fabricated FETs with undoped and Ag^+-doped $CsPbBr_3$ NCs as the semiconducting layer under a bottom-gate, bottom-contact configuration, as shown in Figure 4a. The output and transfer characteristics were measured at room temperature under dark condition. Figure 4b–d presents typical sets of output characteristics [the drain-source current (I_{ds}) vs the drain-source voltage (V_{ds})] for undoped, 0.23% Ag^+-doped, and 0.48% Ag^+-doped $CsPbBr_3$ NCs at gate voltages (V_g) from 60 V to −40 V. The exponential shape of curves indicates that the adoption of short ligands allows the formation of a good-quality Schottky junction between the NCs and electrodes for efficient charge transport (Figure S9). At the same V_g, the I_{ds} values of Ag^+-doped devices are consistently larger than that of the undoped device by several orders of magnitude, demonstrating significantly improved conductivity upon doping. Figure 4e displays the corresponding transfer characteristics tested at V_{ds} = 3 V with the V_g scanning from 60 V to −40 V at a sweep rate of 1 V/s, all of which signify p-type conductivity as I_{ds} increases when V_g decreases (Figure S10). The p-type character becomes more prominent at a higher doping concentration, in line with the band structure deduced from the UPS results. No clear n-type (electron) transport can be obtained from both undoped and Ag^+-doped $CsPbBr_3$ NCs. This suggests that the electron traps may be dominant in the $CsPbBr_3$ NCs, which are probably responsible for the nonradiative recombination in the PL quenching, as also observed in bulk perovskite films.[49] Field effect mobility (μ) can be calculated from the equation[50] $\mu = \frac{dI_{ds}}{dV_{gs}} \cdot \frac{L}{W} \cdot \frac{1}{C_i V_{ds}}$, where W, L, and C_i are the channel width, the channel length, and the gate capacitance per unit area, respectively. For undoped $CsPbBr_3$ NCs, the hole mobility (μ_h) is ~7×10^{-7} $cm^2 V^{-1} s^{-1}$, which is orders of magnitude lower than the μ_h measured in a single $CsPbBr_3$ thin platelet.[51] This evidences that the charge transport in a $CsPbBr_3$-NC film is mainly limited by tunneling of carriers between the $CsPbBr_3$ NCs. However, it is in the same order as that observed in $CsPbBr_3$ polycrystalline films,[51] further confirming that the employment of short ligands does not impede the charge transport between NCs.[18] Remarkably, Ag^+ doping leads to about 3 orders of magnitude higher hole mobility, ~8×10^{-4} $cm^2 V^{-1} s^{-1}$, when the concentration of Ag^+ increases to 0.48%, demonstrating a powerful tunability in the electrical properties of $CsPbBr_3$ NCs.

Considerable improvements of conductivity and hole mobility are clearly associated with the Ag^+ doping, which could be partially attributed to a better energy alignment with Au electrode resulting from the doping-induced upshift of the VBM (Figure S11).[52] However, severe ion migration and phonon scattering effects are known to exist in perovskite semiconducting materials, therefore hampering a further

DOI: 10.1021/acsenergylett.8b02478
ACS Energy Lett. 2019, 4, 534–541

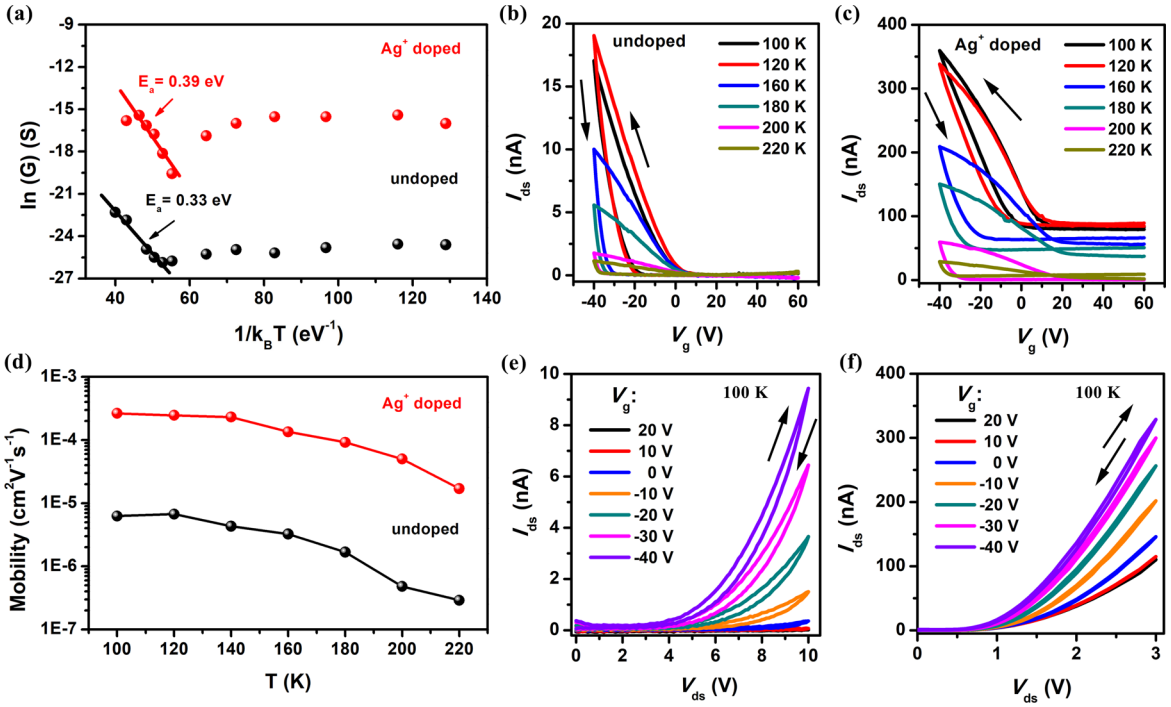

Figure 5. (a) Arrhenius plot of the measured conductance from undoped and Ag^+-doped $CsPbBr_3$ NCs at voltage of 10 V. Transfer characteristics of FETs made of (b) undoped and (c) Ag^+-doped $CsPbBr_3$ NCs measured from 100 to 220 K. The V_{ds} for undoped and Ag^+-doped $CsPbBr_3$ NCs are 10 and 3 V, respectively. (d) Temperature dependence of the FET hole mobility measured for undoped and Ag^+-doped $CsPbBr_3$-NC devices. Output characteristics of (e) undoped and (f) Ag^+-doped $CsPbBr_3$-NC FETs measured at 100 K. The concentration of Ag^+ for doped $CsPbBr_3$ NCs is 0.23%.

understanding of the doping-induced charge-carrier transport mechanism.[23,53] Figure 5a plots the $CsPbBr_3$-NC film conductance (G) versus $1/(k_BT)$ (k_B is Boltzmann's constant) when the temperature (T) increases from 90 K to room temperature (RT). The activation energy (E_a) can be extracted from the Arrhenius plot: $G \propto \exp\left(-\frac{E_a}{k_BT}\right)$.[54] Above ~230 K, both undoped and 0.23% Ag^+-doped $CsPbBr_3$ NCs exhibited a similarly large E_a: ~0.33 eV for undoped NCs and ~0.39 eV for doped NCs, indicating the presence of ion migration. Below ~230 K, the conductance variation becomes much smaller, suggesting that the ion migration is largely suppressed in this temperature regime.[51] As a result, we performed temperature-dependent FET studies below 220 K for undoped and 0.23% Ag^+-doped $CsPbBr_3$ NCs to effectively reduce the ion screening effect in order to establish a direct correlation between Ag^+ doping and the charge-carrier transport mechanism. Figure 5b,c shows the transfer characteristics of undoped and Ag^+-doped $CsPbBr_3$-NC FETs measured from 100 to 220 K. The corresponding μ_h versus temperature curves are plotted in Figure 5d. The mobility progressively increases with decreasing temperature and saturated at ~100 K when phonon scattering effect is also eliminated.[23,55] Figure 5e,f displays typical output characteristics of FETs measured at 100 K. Though with similar temperature dependency, Ag^+-doped $CsPbBr_3$ NCs exhibit about two orders-of-magnitude higher field effect mobility compared with undoped $CsPbBr_3$ NCs. This further confirms Ag^+-doping should dominantly contribute to the conductivity and hole mobility improvement at RT. Intriguingly, FETs made from Ag^+-doped NCs demonstrate negligible hysteresis, suggesting that Ag^+ doping could effectively reduce the density of hole traps in the perovskite NCs.

In summary, we report for the first time a successful controlled heterovalent doping of Ag^+ in substitution of Pb^{2+} in colloidal $CsPbBr_3$ NCs via a simple room-temperature synthesis method. The Ag^+ doping has demonstrated a great potential in modulating the electrical properties of $CsPbBr_3$ NCs. UPS results suggest that as an electrically active impurity in $CsPbBr_3$ NCs, Ag^+ induces impurity levels close to the valence band and shifts the Fermi level down toward the valence band, thereby giving rise to a well-defined p-type doping. It is found that undoped $CsPbBr_3$ NCs exhibit poor electrical conductivity and very low charge-carrier mobility. After Ag^+ doping, significant improvement of both the conductivity and charge-carrier mobility by nearly 3 orders of magnitude has been achieved. Low-temperature (<230 K) FET studies further confirm the dominant contribution of Ag^+ doping to charge-carrier transport by suppressing the influence of ion transport and phonon screening. This work demonstrates the remarkable tunability of heterovalent doping on the electrical properties of halide perovskite NCs.

■ ASSOCIATED CONTENT

Supporting Information

The Supporting Information is available free of charge on the ACS Publications website at DOI: 10.1021/acsenergylett.8b02478.

Experimental methods, TEM images, GIWAXS patterns, XPS results, TRPL results of undoped and Ag^+-doped $CsPbBr_3$ NCs, Tauc plots of the optical absorption spectra of undoped and Ag^+-doped $CsPbBr_3$ NCs, STM image of the FTO substrate, STS spectra collected from undoped and Ag^+-doped $CsPbBr_3$ NCs, FET results of undoped $CsPbBr_3$ NCs after washing, gate leakage

DOI: 10.1021/acsenergylett.8b02478
ACS Energy Lett. 2019, 4, 534−541

current for the FETs fabricated with Ag^+-doped NCs, and band diagrams of the interface between the Au electrode and $CsPbBr_3$ NCs (PDF)

AUTHOR INFORMATION

Corresponding Author

*E-mail: xhlu@phy.cuhk.edu.hk.

ORCID

Yaping Ma: 0000-0003-3907-6881
Yao-Jane Hsu: 0000-0001-7687-4351
Ni Zhao: 0000-0002-1536-8516
Jianbin Xu: 0000-0003-0509-9508
Xinhui Lu: 0000-0002-1908-3294

Notes

The authors declare no competing financial interest.

ACKNOWLEDGMENTS

We are grateful for the beam time and technical support provided by 23A SWAXS and BL09A2 U5 beamline at NSRRC, Hsinchu. We acknowledge the financial support from Research Grant Council of Hong Kong (General Research Fund No. 24306318, CUHK Direct Grant). We thank Dr. Wing Fat Chan, Department of Chemistry of CUHK for providing ICP-OES measurements.

REFERENCES

(1) Green, M. A.; Ho, B. A.; Snaith, H. J. The Emergence of Perovskite Solar Cells. *Nat. Photonics* **2014**, *8*, 506−514.

(2) Burschka, J.; Pellet, N.; Moon, S. J.; Humphry, B. R.; Gao, P.; Nazeeruddin, M. K.; Gratzel, M. Sequential Deposition as a Route to High-Performance Perovskite-Sensitized Solar Cells. *Nature* **2013**, *499*, 316−319.

(3) Kojima, A.; Teshima, K.; Shirai, Y.; Miyasaka, T. Organometal Halide Perovskites as Visible-Light Sensitizers for Photovoltaic Cells. *J. Am. Chem. Soc.* **2009**, *131*, 6050−6051.

(4) Manser, J. S.; Christians, J. A.; Kamat, P. V. Intriguing Optoelectronic Properties of Metal Halide Perovskites. *Chem. Rev.* **2016**, *116*, 12956−13008.

(5) Sutherland, B. R.; Sargent, E. H. Perovskite Photonic Sources. *Nat. Photonics* **2016**, *10*, 295−302.

(6) Zhang, X.; Lin, H.; Huang, H.; Reckmeier, C.; Zhang, Y.; Choy, W. C. H.; Rogach, A. L. Enhancing the Brightness of Cesium Lead Halide Perovskite Nanocrystal Based Green Light-Emitting Devices through the Interface Engineering with Perfluorinated Ionomer. *Nano Lett.* **2016**, *16*, 1415−1420.

(7) Li, F.; Ma, C.; Wang, H.; Hu, W.; Yu, W.; Sheikh, A. D.; Wu, T. Ambipolar Solution-Processed Hybrid Perovskite Phototransistors. *Nat. Commun.* **2015**, *6*, 8238−8245.

(8) Chen, Q.; Wu, J.; Ou, X.; Huang, B.; Almutlaq, J.; Zhumekenov, A. A.; Guan, X.; Han, S.; Liang, L.; Yi, Z.; et al. All-Inorganic Perovskite Nanocrystal Scintillators. *Nature* **2018**, *561*, 88−93.

(9) Li, J.; Xu, L.; Wang, T.; Song, J.; Chen, J.; Xue, J.; Dong, Y.; Cai, B.; Shan, Q.; Han, B.; et al. 50-Fold EQE Improvement up to 6.27% of Solution-Processed All-Inorganic Perovskite $CsPbBr_3$ QLEDs via Surface Ligand Density Control. *Adv. Mater.* **2017**, *29*, 1603885.

(10) Wang, N.; Cheng, L.; Ge, R.; Zhang, S.; Miao, Y.; Zou, W.; Yi, C.; Sun, Y.; Cao, Y.; Yang, R.; et al. Perovskite Light-Emitting Diodes Based on Solution-Processed Self-Organized Multiple Quantum Wells. *Nat. Photonics* **2016**, *10*, 699−704.

(11) Huang, H.; Bodnarchuk, M. I.; Kershaw, S. V.; Kovalenko, M. V.; Rogach, A. L. Lead Halide Perovskite Nanocrystals in the Research Spotlight: Stability and Defect Tolerance. *ACS Energy Lett.* **2017**, *2*, 2071−2083.

(12) Akkerman, Q. A.; Rainò, G.; Kovalenko, M. V.; Manna, L. Genesis, Challenges and Opportunities for Colloidal Lead Halide Perovskite Nanocrystals. *Nat. Mater.* **2018**, *17*, 394−405.

(13) Protesescu, L.; Yakunin, S.; Bodnarchuk, M. I.; Krieg, F.; Caputo, R.; Hendon, C. H.; Yang, R. X.; Walsh, A.; Kovalenko, M. V. Nanocrystals of Cesium Lead Halide Perovskites ($CsPbX_3$, X = Cl, Br, and I): Novel Optoelectronic Materials Showing Bright Emission with Wide Color Gamut. *Nano Lett.* **2015**, *15*, 3692−3696.

(14) Zhang, F.; Zhong, H.; Chen, C.; Wu, X. G.; Hu, X.; Huang, H.; Han, J.; Zou, B.; Dong, Y. Brightly Luminescent and Color-Tunable Colloidal $CH_3NH_3PbX_3$ (X = Br, I, Cl) Quantum Dots: Potential Alternatives for Display Technology. *ACS Nano* **2015**, *9*, 4533−4542.

(15) Wang, L.; Williams, N. E.; Malachosky, E. W.; Otto, J. P.; Hayes, D.; Wood, R. E.; Guyot, S. P.; Engel, G. S. Scalable Ligand-Mediated Transport Synthesis of Organic−Inorganic Hybrid Perovskite Nanocrystals with Resolved Electronic Structure and Ultrafast Dynamics. *ACS Nano* **2017**, *11*, 2689−2696.

(16) Lamberti, F.; Litti, L.; De Bastiani, M.; Sorrentino, R.; Gandini, M.; Meneghetti, M.; Petrozza, A. High-Quality, Ligands-Free, Mixed-Halide Perovskite Nanocrystals Inks for Optoelectronic Applications. *Adv. Energy Mater.* **2017**, *7*, 1601703.

(17) Naphade, R.; Nagane, S.; Shanker, G. S.; Fernandes, R.; Kothari, D.; Zhou, Y.; Padture, N. P.; Ogale, S. Hybrid Perovskite Quantum Nanostructures Synthesized by Electrospray Antisolvent-Solvent Extraction and Intercalation. *ACS Appl. Mater. Interfaces* **2016**, *8*, 854−861.

(18) Xiao, Z.; Kerner, R. A.; Zhao, L.; Tran, N. L.; Lee, K. M.; Koh, T. W.; Scholes, G. D.; Rand, B. P. Efficient Perovskite Light-Emitting Diodes Featuring Nanometre-Sized Crystallites. *Nat. Photonics* **2017**, *11*, 108−115.

(19) Lu, M.; Zhang, X.; Bai, X.; Wu, H.; Shen, X.; Zhang, Y.; Zhang, W.; Zheng, W.; Song, H.; Yu, W. W.; et al. Spontaneous Silver Doping and Surface Passivation of $CsPbI_3$ Perovskite Active Layer Enable Light-Emitting Devices with an External Quantum Efficiency of 11.2%. *ACS Energy Lett.* **2018**, *3*, 1571−1577.

(20) Sanehira, E. M.; Marshall, A. R.; Christians, J. A.; Harvey, S. P.; Ciesielski, P. N.; Wheeler, L. M.; Schulz, P.; Lin, L. Y.; Beard, M. C.; Luther, J. M. Enhanced Mobility $CsPbI_3$ Quantum Dot Arrays for Record-Efficiency, High-Voltage Photovoltaic Cells. *Sci. Adv.* **2017**, *3*, No. eaao4204.

(21) Xu, Y. F.; Yang, M. Z.; Chen, B. X.; Wang, X. D.; Chen, H. Y.; Kuang, D. B.; Su, C. Y. A $CsPbBr_3$ Perovskite Quantum Dot/Graphene Oxide Composite for Photocatalytic CO_2 Reduction. *J. Am. Chem. Soc.* **2017**, *139*, 5660−5663.

(22) Stoeckel, M. A.; Gobbi, M.; Bonacchi, S.; Liscio, F.; Ferlauto, L.; Orgiu, E.; Samorì, P. Reversible, Fast, and Wide-Range Oxygen Sensor Based on Nanostructured Organometal Halide Perovskite. *Adv. Mater.* **2017**, *29*, 1702469.

(23) Senanayak, S. P.; Yang, B.; Thomas, T. H.; Giesbrecht, N.; Huang, W.; Gann, E.; Nair, B.; Goedel, K.; Guha, S.; Moya, X.; et al. Understanding Charge Transport in Lead Iodide Perovskite Thin-Film Field-Effect Transistors. *Sci. Adv.* **2017**, *3*, No. e1601935.

(24) Kagan, C. R.; Mitzi, D. B.; Dimitrakopoulos, C. D. Organic-Inorganic Hybrid Materials as Semiconducting Channels in Thin-Film Field-Effect Transistors. *Science* **1999**, *286*, 945−947.

(25) Chin, X. Y.; Cortecchia, D.; Yin, J.; Bruno, A.; Soci, C. Lead Iodide Perovskite Light-Emitting Field-Effect Transistor. *Nat. Commun.* **2015**, *6*, 7383.

(26) Swarnkar, A.; Ravi, V. K.; Nag, A. Beyond Colloidal Cesium Lead Halide Perovskite Nanocrystals: Analogous Metal Halides and Doping. *ACS Energy Lett.* **2017**, *2*, 1089−1098.

(27) Abdelhady, A. L.; Saidaminov, M. I.; Murali, B.; Adinolfi, V.; Voznyy, O.; Katsiev, K.; Alarousu, E.; Comin, R.; Dursun, I.; Sinatra, L.; et al. Heterovalent Dopant Incorporation for Bandgap and Type Engineering of Perovskite Crystals. *J. Phys. Chem. Lett.* **2016**, *7*, 295−301.

(28) Zhou, Y.; Chen, J.; Bakr, O. M.; Sun, H. T. Metal-Doped Lead Halide Perovskites: Synthesis, Properties, and Optoelectronic Applications. *Chem. Mater.* **2018**, *30*, 6589−6613.

DOI: 10.1021/acsenergylett.8b02478
ACS Energy Lett. 2019, 4, 534−541

(29) Parobek, D.; Roman, B. J.; Dong, Y.; Jin, H.; Lee, E.; Sheldon, M.; Son, D. H. Exciton-to-Dopant Energy Transfer in Mn-Doped Cesium Lead Halide Perovskite Nanocrystals. *Nano Lett.* **2016**, *16*, 7376−7380.
(30) van der Stam, W.; Geuchies, J. J.; Altantzis, T.; van den Bos, K. H. W.; Meeldijk, J. D.; Van Aert, S.; Bals, S.; Vanmaekelbergh, D.; de Mello Donega, C. Highly Emissive Divalent-Ion-Doped Colloidal $CsPb_{1-x}M_xBr_3$ Perovskite Nanocrystals through Cation Exchange. *J. Am. Chem. Soc.* **2017**, *139*, 4087−4097.
(31) Liu, W.; Lin, Q.; Li, H.; Wu, K.; Robel, I.; Pietryga, J. M.; Klimov, V. I. Mn^{2+}-Doped Lead Halide Perovskite Nanocrystals with Dual-Color Emission Controlled by Halide Content. *J. Am. Chem. Soc.* **2016**, *138*, 14954−14961.
(32) Liu, H.; Wu, Z.; Shao, J.; Yao, D.; Gao, H.; Liu, Y.; Yu, W.; Zhang, H.; Yang, B. $CsPb_xMn_{1-x}Cl_3$ Perovskite Quantum Dots with High Mn Substitution Ratio. *ACS Nano* **2017**, *11*, 2239−2247.
(33) Begum, R.; Parida, M. R.; Abdelhady, A. L.; Murali, B.; Alyami, N. M.; Ahmed, G. H.; Hedhili, M. N.; Bakr, O. M.; Mohammed, O. F. Engineering Interfacial Charge Transfer in $CsPbBr_3$ Perovskite Nanocrystals by Heterovalent Doping. *J. Am. Chem. Soc.* **2017**, *139*, 731−737.
(34) Liu, M.; Zhong, G.; Yin, Y.; Miao, J.; Li, K.; Wang, C.; Xu, X.; Shen, C.; Meng, H. Aluminum-Doped Cesium Lead Bromide Perovskite Nanocrystals with Stable Blue Photoluminescence Used for Display Backlight. *Adv. Sci.* **2017**, *4*, 1700335.
(35) Pan, G.; Bai, X.; Yang, D.; Chen, X.; Jing, P.; Qu, S.; Zhang, L.; Zhou, D.; Zhu, J.; Xu, W.; et al. Doping Lanthanide into Perovskite Nanocrystals: Highly Improved and Expanded Optical Properties. *Nano Lett.* **2017**, *17*, 8005−8011.
(36) Yao, J. S.; Ge, J.; Han, B. N.; Wang, K. H.; Yao, H. B.; Yu, H. L.; Li, J. H.; Zhu, B. S.; Song, J. Z.; Chen, C.; et al. Ce^{3+}-Doping to Modulate Photoluminescence Kinetics for Efficient $CsPbBr_3$ Nanocrystals Based Light-Emitting Diodes. *J. Am. Chem. Soc.* **2018**, *140*, 3626−3634.
(37) Chen, Q.; Chen, L.; Ye, F.; Zhao, T.; Tang, F.; Rajagopal, A.; Jiang, Z.; Jiang, S.; Jen, A. K. Y.; Xie, Y.; et al. Ag-Incorporated Organic−Inorganic Perovskite Films and Planar Heterojunction Solar Cells. *Nano Lett.* **2017**, *17*, 3231−3237.
(38) Kang, M. S.; Sahu, A.; Frisbie, C. D.; Norris, D. J. Influence of Silver Doping on Electron Transport in Thin Films of PbSe Nanocrystals. *Adv. Mater.* **2013**, *25*, 725−731.
(39) Akkerman, Q. A.; Gandini, M.; Di Stasio, F.; Rastogi, P.; Palazon, F.; Bertoni, G.; Ball, J. M.; Prato, M.; Petrozza, A.; Manna, L. Strongly Emissive Perovskite Nanocrystal Inks for High-Voltage Solar Cells. *Nat. Energy* **2017**, *2*, 16194.
(40) Yang, Y.; Jin, Y.; He, H.; Wang, Q.; Tu, Y.; Lu, H.; Ye, Z. Dopant-Induced Shape Evolution of Colloidal Nanocrystals: The Case of Zinc Oxide. *J. Am. Chem. Soc.* **2010**, *132*, 13381−13394.
(41) Mai, J.; Xiao, Y.; Zhou, G.; Wang, J.; Zhu, J.; Zhao, N.; Zhan, X.; Lu, X. Hidden Structure Ordering Along Backbone of Fused-Ring Electron Acceptors Enhanced by Ternary Bulk Heterojunction. *Adv. Mater.* **2018**, *30*, 1802888.
(42) Stavrinadis, A.; Rath, A. K.; de Arquer, F. P. G.; Diedenhofen, S. L.; Magén, C.; Martinez, L.; So, D.; Konstantatos, G. Heterovalent Cation Substitutional Doping for Quantum Dot Homojunction Solar Cells. *Nat. Commun.* **2013**, *4*, 2981.
(43) Sahu, A.; Kang, M. S.; Kompch, A.; Notthoff, C.; Wills, A. W.; Deng, D.; Winterer, M.; Frisbie, C. D.; Norris, D. J. Electronic Impurity Doping in CdSe Nanocrystals. *Nano Lett.* **2012**, *12*, 2587−2594.
(44) Liu, M.; Yao, W.; Li, C.; Wu, Z.; Li, L. Tuning Emission and Stokes Shift of CdS Quantum Dots via Copper and Indium Co-doping. *RSC Adv.* **2015**, *5*, 628−634.
(45) Brennan, M. C.; Zinna, J.; Kuno, M. Existence of a Size-Dependent Stokes Shift in $CsPbBr_3$ Perovskite Nanocrystals. *ACS Energy Lett.* **2017**, *2*, 1487−1488.
(46) Filip, M. R.; Hillman, S.; Haghighirad, A. A.; Snaith, H. J.; Giustino, F. Band Gaps of the Lead-Free Halide Double Perovskites $Cs_2BiAgCl_6$ and $Cs_2BiAgBr_6$ from Theory and Experiment. *J. Phys. Chem. Lett.* **2016**, *7*, 2579−2585.
(47) Shahbazi, S.; Tsai, C. M.; Narra, S.; Wang, C. Y.; Shiu, H. S.; Afshar, S.; Taghavinia, N.; Diau, E. W. G. Ag Doping of Organometal Lead Halide Perovskites: Morphology Modification and P-Type Character. *J. Phys. Chem. C* **2017**, *121*, 3673−3679.
(48) Abdi-Jalebi, M.; Pazoki, M.; Philippe, B.; Dar, M. I.; Alsari, M.; Sadhanala, A.; Divitini, G.; Imani, R.; Lilliu, S.; Kullgren, J.; et al. Dedoping of Lead Halide Perovskites Incorporating Monovalent Cations. *ACS Nano* **2018**, *12*, 7301−7311.
(49) Wetzelaer, A. H.; Scheepers, M.; Sempere, A. M.; Momblona, C.; Avila, J.; Bolink, H. J. Trap-Assisted Non-Radiative Recombination in Organic-Inorganic Perovskite Solar Cells. *Adv. Mater.* **2015**, *27*, 1837−1841.
(50) Hu, X.; Zhou, H.; Jiang, Z.; Wang, X.; Yuan, S.; Lan, J.; Fu, Y.; Zhang, X.; Zheng, W.; Wang, X.; et al. Direct Vapor Growth of Perovskite $CsPbBr_3$ Nanoplate Electroluminescence Devices. *ACS Nano* **2017**, *11*, 9869−9876.
(51) Huo, C.; Liu, X.; Song, X.; Wang, Z.; Zeng, H. Field-Effect Transistors Based on Vander-Waals-Grown and Dry-Transferred All-Inorganic Perovskite Ultrathin Platelets. *J. Phys. Chem. Lett.* **2017**, *8*, 4785−4792.
(52) Tung, R. T. The Physics and Chemistry of The Schottky Barrier Height. *Appl. Phys. Rev.* **2014**, *1*, 011304.
(53) Eames, C.; Frost, J. M.; Barnes, P. R. F.; O'Regan, B. C.; Walsh, A.; Islam, M. S. Ionic Transport in Hybrid Lead Iodide Perovskite Solar Cells. *Nat. Commun.* **2015**, *6*, 7497.
(54) Zhao, Y. C.; Zhou, W. K.; Zhou, X.; Liu, K. H.; Yu, D. P.; Zhao, Q. Quantification of Light-Enhanced Ionic Transport in Lead Iodide Perovskite Thin Films and Its Solar Cell Applications. *Light: Sci. Appl.* **2016**, *6*, No. e16243.
(55) Li, D.; Wang, G.; Cheng, H. C.; Chen, C. Y.; Wu, H.; Liu, Y.; Huang, Y.; Duan, X. Size-Dependent Phase Transition in Methylammonium Lead Iodide Perovskite Microplate Crystals. *Nat. Commun.* **2016**, *7*, 11330.

DOI: 10.1021/acsenergylett.8b02478
ACS Energy Lett. 2019, 4, 534−541